metals

MDPI

Article

Cooling-Rate Effect on Microstructure and Mechanical Properties of $Al_{0.5}CoCrFeNi$ High-Entropy Alloy

Ke Xiong [1,2], Lin Huang [1,2,*], Xiaofeng Wang [1,2], Lin Yu [1,3] and Wei Feng [1,2,*]

[1] School of Mechanical Engineering, Chengdu University, Chengdu 610106, China; xiongke@stu.cdu.edu.cn (K.X.); 13880073327@163.com (X.W.); 13658066449@163.com (L.Y.)
[2] Sichuan Province Engineering Technology Research Center of Powder Metallurgy, Chengdu 610106, China
[3] Sichuan Yiran Material Technology Co., Ltd., Chengdu 610100, China
* Correspondence: huanglin@cdu.edu.cn (L.H.); fengwei@cdu.edu.cn (W.F.)

Abstract: $Al_{0.5}CoCrFeNi$ high-entropy alloy (HEA) was prepared by spark plasma sintering (SPS) using $Al_{0.5}CoCrFeNi$ gas atomized powder and was treated with different cooling rates (furnace cooling, air cooling, water quenching). The phase composition, microstructure, tensile properties, Vickers hardness, compactness, and fracture morphology of the alloy were systematically studied. The results show that the cooling rate can change the phase composition and phase shape of $Al_{0.5}CoCrFeNi$ HEA from BCC + FCC phase to BCC + FCC + B2 phase, and the BCC phase coarsens. The ultimate tensile strength and yield strength of the heat-treated $Al_{0.5}CoCrFeNi$ HEA decreased with increasing cooling rate, but elongation and Vickers hardness increased with increasing cooling rate. The ultimate tensile strength and yield strength of the furnace cooling (FC) samples reached the maximum value of 985.2 MPa and 524.1 MPa, respectively. The elongation and hardness of the water quenching (WQ) samples reached a maximum value of 43.1% and 547.3 HV, respectively, and the compactness of the alloy is higher than 98.8%. Therefore, the properties of Al0.5CoCrFeNi HEAs can be greatly improved by treatment with different cooling rates.

Keywords: $Al_{0.5}CoCrFeNi$ HEA; spark plasma sintering; cooling rate; microstructure; mechanical properties

Citation: Xiong, K.; Huang, L.; Wang, X.; Yu, L.; Feng, W. Cooling-Rate Effect on Microstructure and Mechanical Properties of $Al_{0.5}CoCrFeNi$ High-Entropy Alloy. *Metals* **2022**, *12*, 1254. https://doi.org/10.3390/met12081254

Academic Editor: Babak Shalchi Amirkhiz

Received: 27 June 2022
Accepted: 22 July 2022
Published: 26 July 2022

1. Introduction

As a new type of special metal material, high-entropy alloys (HEAs) have five or more elements in near-equiatomic concentrations [1], and their mixed configuration entropy is large [2], thus forming a simple, solid solution structure of face-centered cubic (FCC), body-centered cubic (BCC), or hexagonal dense reactor (HCP) [3–5]. These alloys have many excellent properties and have attracted extensive attention in recent years [6–15].

Compared with other HEAs (CoCrFeNiMn, etc.), AlCoCrFeNi HEA has good mechanical properties, oxidation resistance, and corrosion resistance [16–21]. At present, AlCoCrFeNi HEA is usually prepared by arc melting or casting [22], and its microstructure consists of an FCC phase rich in Co and Fe elements, BCC phase rich in Cr elements, and ordered B2 phase rich in Al and Ni elements [23]. However, during the solidification of the alloy, the formation of compositional segregation can lead to a decrease in its mechanical properties [18,24,25]. At the same time, the preparation of HEA by vacuum arc melting technology requires higher energy, and the cost is high, and the shape and size of the product are limited [26,27]. However, samples prepared by powder metallurgy (PM) methods, such as spark plasma sintering (SPS), have more uniform compositions, high densities, and finer grain sizes, and their properties are also better, avoiding or reducing metalworking and removal processes, thereby greatly reducing damage to the synthesized AlCoCrFeNi HEA [28–35].

Vikas et al. [36] prepared AlCoCrFeNi HEA pre-alloyed powder by high-energy ball milling (HEBM) mixed element raw powder. The ball milling time is long (up to 30 h

or even longer), and the ball-milled pre-alloyed powder will be subjected to grinding media and environmental pollution, and the order of addition of metal elements can also affect the formation of HEA phase [35,37]. The AlCoCrFeNi HEA powder prepared by Kunce et al. [38] by gas atomization has higher purity and more uniform alloying element composition, which is a more ideal pre-alloyed powder for preparing HEA bulk [39].

$Al_xCoCrFeNi$, as a typical HEA system, can obtain a single-phase or multi-phase structure by controlling the atomic percentage of Al [40]. Among them, the sintering temperature of $Al_{0.5}CoCrFeNi$ HEA is higher than 800 °C [41], which presents a BCC + FCC two-phase structure alloy, which has high plasticity and high strength and has a broader prospect than single-phase alloys. At present, most studies only focus on the properties of $Al_{0.5}CoCrFeNi$ as cast or sintered alloys. It is known that the energy barrier of phase transformation can be overcome by heat treatment, and the cooling rate of the alloy can change its microstructure [42]. Thus, it is of great significance to study the effect of heat treatment, especially the cooling rate, on the microstructure and mechanical properties of $Al_{0.5}CoCrFeNi$. Therefore, the effect of cooling rate on the microstructure and mechanical properties of $Al_{0.5}CoCrFeNi$ HEA was systematically studied in this paper.

2. Materials and Methods

2.1. $Al_{0.5}CoCrFeNi$ High-Entropy Alloy Powder

In this work, powder of $Al_{0.5}CoCrFeNi$ HEA was prepared by gas atomization under argon atmosphere with high-purity Al, Co, Cr, Fe, and Ni (purities higher than 99.9 wt.%). The powder particle size is 10~25 μm and was purchased from Jiangsu Vilory Advanced Materials Technology Co., Ltd. (Jiangsu, China). Figure 1 shows the microstructure of $Al_{0.5}CoCrFeNi$ HEA powder. It can be seen from Figure 1 that the majority of powders were spherical, and the surface of the atomized powders was relatively smooth. A small amount of non-spherical particles with small particles (satellites) attached were also found in Figure 1 [43]. Due to the small size and fast solidification speed of satellite particles, the solidified satellite particles will splash out under the action of atomized gas. Since larger particles take more time to solidify than finer particles (satellites), spattering satellite particles collide with larger powder particles. Thus, satellite particles will combine with large powders to form irregular particles [44]. Satellite particles will reduce powder bluntness and increase particle size; this is also a significant factor affecting the property of the powder, especially powder flowability [45].

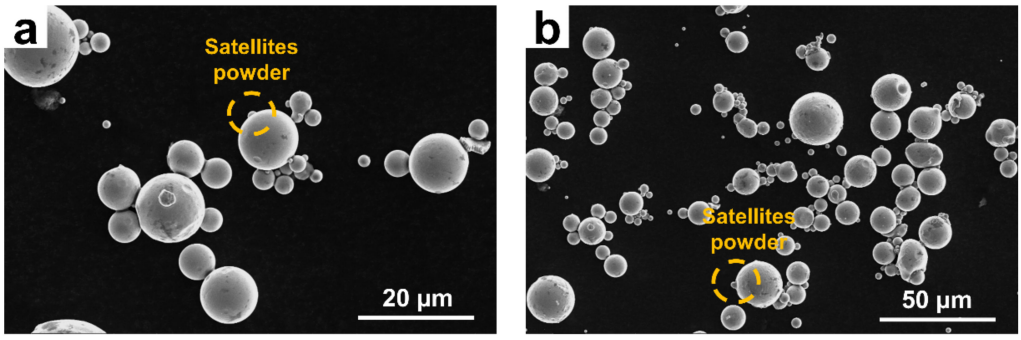

Figure 1. SEM of $Al_{0.5}CoCrFeNi$ HEA powder. (**a**) 20 μm, (**b**) 50 μm.

2.2. $Al_{0.5}CoCrFeNi$ High-Entropy Alloy Prepared by Spark Plasma Sintering

The $Al_{0.5}CoCrFeNi$ HEA gas-atomized powder was consolidated with a LABOX-350 spark plasma sintering machine (SPS, SINTER LAND INC., Chiyo, Japan) under a constant axial pressure of 30 MPa and then heated to 1050 °C at a certain heating rate (below 900 °C, the heating rate is 50 °C/min; above 900 °C, the heating rate is 25 °C/min), and the temperature was kept for 10 min to prepare a cylindrical sample with a diameter of 30 mm and a thickness of about 10 mm.

2.3. Heat Treatments

The sintered samples were heated in a KSL-1400-A3 high-temperature furnace (Hefei Kejing Material Technology Co., Ltd., Hefei, China) at 1100 °C. (The σ phase of AlCoCrFeNi alloy can be formed at around 600 °C. The transformation from BCC phase to σ phase will occur at around 650 °C, and it will be transformed back to BCC phase at around 950 °C [46]. The homogenization effect is achieved at 1100 °C [47]) The initial temperature of samples is 30 °C, and the heating rate is 10 °C/min, and the holding time is 3 h at 1100 °C. (According to the study of Munitz et al. [46], 3 h is enough for the sample to be homogenized) The samples were then cooled by the different methods of furnace cooling (FC), air cooling (AC), and water quenching (WQ). The cooling rates of the three different cooling methods are: 0.02~0.03 °C/s (FC), 0.9~1.8 °C/s (AC), and >75 °C/s (WQ).

2.4. Microstructural and Mechanical Property Characterization

Tensile specimens and damping specimens were prepared by a DK7735 CNC wire-cutting machine (Taizhou Weihai CNC Machine Tool Co., Ltd., Taizhou, China). The sample phase analysis was carried out using the DX-2500 X-ray diffraction (XRD, Dandong Haoyuan Instrument Co. Ltd., Dandong, China). Test conditions: Cu target Kα ray, tube voltage of 40 kV, tube current of 40 mA, scanning angle range of 20~90°, step angle of 0.06°/s, and sampling time of 0.5 s. The surface micro-morphology was determined by the Quanta 450 FEG field emission scanning electron microscope (FEI Company, Hillsboro, OR, USA). The room temperature tensile test was carried out by using ETM-105D universal testing machine (Shenzhen Wance Test Equipment Co., Ltd., Shenzhen, China). Test conditions: the original gauge length of the tensile specimen was 5 mm, the cross-sectional area was 1.5 mm × 1 mm, and the tensile rate was 0.2 mm/min. To avoid errors, five samples were tested for each alloy. The hardness of the samples was measured by MHVD-50AP Vickers hardness tester (Shanghai Jujing Precision Instrument Co., Ltd., Shanghai, China); the fixed load was 5 kg, the holding time was 15 s, and the average value of 7 points was measured for each sample. Compactness of alloys was determined as the ratio of density to theoretical density, and density of alloys was measured based on the Archimedes method.

3. Results and Discussion

3.1. Microstructure

Figure 2 is the XRD pattern of $Al_{0.5}$CoCrFeNi HEA. As shown in Figure 1a, $Al_{0.5}$CoCrFeNi powder has a dual-phase structure of BCC + FCC. After SPS, it can be clearly found that the BCC phase transitions to the FCC phase. The formation of the FCC phase is related to the critical condition of the non-equilibrium process of fast sintering in the SPS process, and the large pulse current of the SPS may also lead to the uncertain transition of the phase [48]. B2, BCC, and FCC phases appear in the alloys after heat treatment, which are different from the microstructure of sintered $Al_{0.5}$CoCrFeNi HEA, in which FCC and BCC phases coexist [49]. Compared with the sintered state, the FCC diffraction peak intensity of the heat-treated samples decreased, and the BCC and B2 diffraction peak intensities increased, indicating that the heat treatment caused part of the FCC phase to transform into the BCC and B2 phases [50]. Figure 2b is an enlarged XRD pattern near 44°. It can be seen that compared with the sintered state (SS), the diffraction peak of the (111) crystal plane of the heat-treated sample shifted to a high angle, resulting in a decrease in the interplanar spacing [51], which is the exclusion of Al atoms with larger atomic radii from the matrix, thereby releasing the distortion energy, indicating that heat treatment can reduce lattice distortion [1].

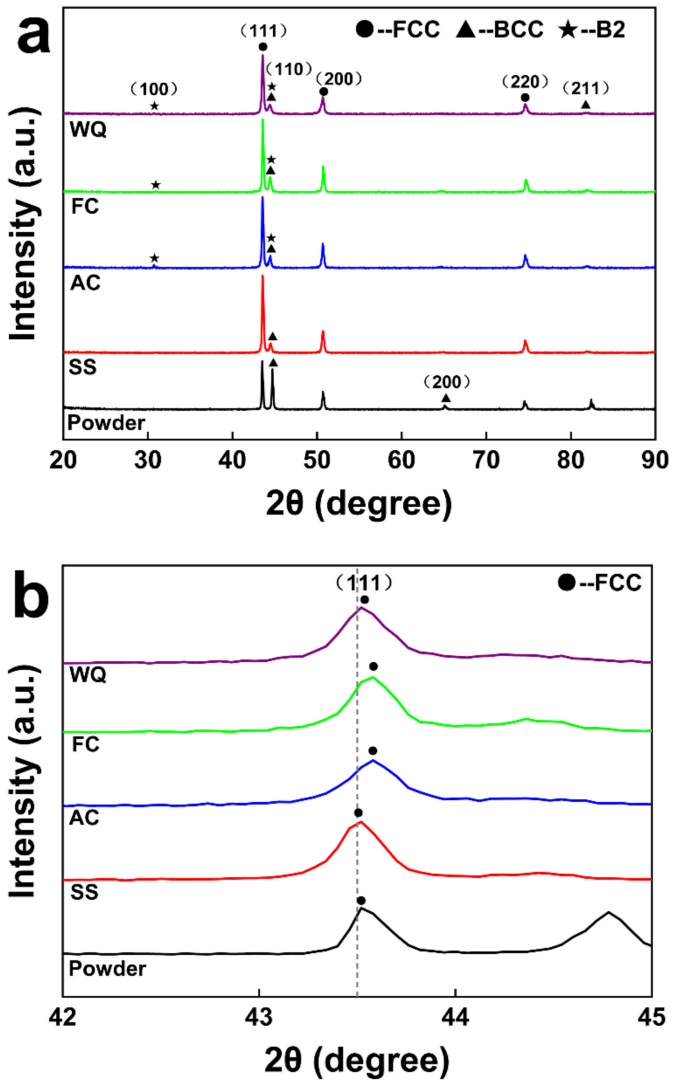

Figure 2. XRD patterns of the samples: (**a**) XRD patterns of $Al_{0.5}CoCrFeNi$ HEA (powder, SS, FC, AC, WQ); (**b**) XRD patterns of amplified peaks near 44°.

Figure 3 depicts SEM images of $Al_{0.5}CoCrFeNi$ HEA as sintered and treated with different cooling rates. It can be seen that some very small voids (black dots in Figure 3) can be observed on the surface of the sample, which is due to the inhomogeneity of the current during the SPS sintering process, which makes the local current density at the sintering neck large, the temperature too high, and the powder volatile, thus forming micropores at higher sintering temperatures [19]. The SS consists of FCC and BCC phases, while the heat-treated samples consist of FCC, BCC, and B2 phases. The B2 phase of the FC sample is needle-like. With the increase of cooling rate, the volume of the B2 phase of the AC and WQ samples increases obviously, and it is strip-shaped [52]. Compared with the sintered state, the FCC phase of the heat-treated sample was reduced, and the BCC was obviously aggregated and coarsened, and the volume of the BCC phase of the water-cooled sample was the largest. It shows that the increase of cooling rate can accelerate the transformation of FCC phase to BCC phase and B2 phase.

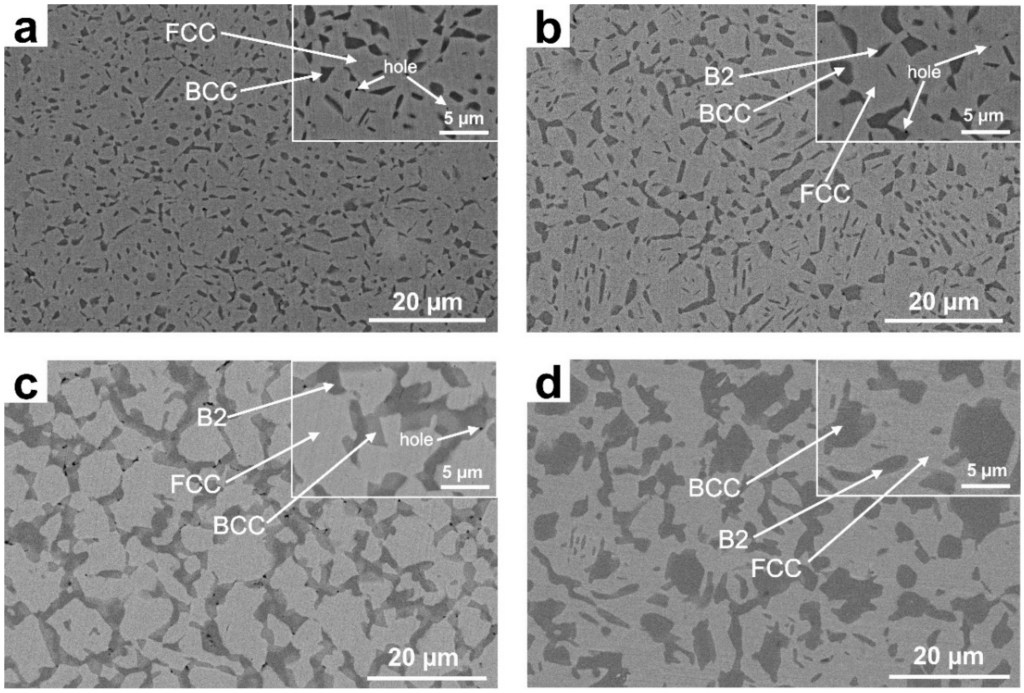

Figure 3. SEM images of $Al_{0.5}CoCrFeNi$ HEA as-sintered and treated with different cooling rates: (**a**) SS; (**b**) FC; (**c**) AC; (**d**) WQ.

Table 1 shows the element content results of different phases. Combined with the SEM image in Figure 3 and the EDS analysis results in Table 1, it shows that the FCC phase is rich in Fe, Co, and Ni elements; the BCC phase is rich in Cr elements, and the Cr content of the BCC phase in the sintered sample is 43%, and the BCC phase in the heat-treated sample is 43%; the content of Cr element increased significantly: all higher than 55%. The B2 phase is rich in Al and Ni elements, which is consistent with previous reports [53].

Table 1. EDS analysis results (in at%) of $Al_{0.5}CoCrFeNi$ HEA micro-domains in the sintered state and treated with different cooling rates; see Figure 3 for the specific phases.

Al0.5CoCrFeNi	Phase	Chemical Composition/at.%				
		Al	Co	Cr	Fe	Ni
Sintered state	FCC	9.39	24.01	20.73	23.77	22.09
	BCC	12.56	12.77	43.20	13.04	18.43
Furnace cooling	FCC	6.92	22.90	20.19	26.08	23.91
	BCC	2.72	11.72	61.98	17.50	6.08
	B2	29.12	16.38	9.98	12.01	32.51
Air cooling	FCC	9.26	26.52	13.17	26.94	24.11
	BCC	2.66	5.63	78.71	9.38	3.63
	B2	28.12	19.28	5.12	15.31	32.16
Water quenching	FCC	10.03	29.90	5.42	28.94	25.71
	BCC	2.42	13.93	54.39	24.23	5.03
	B2	31.27	5.31	10.41	16.41	36.60

The surface scan results of the AC samples in Figure 4 further prove the element segregation effect of the FCC phase, BCC phase, and B2 phase. This phase segregation effect occurs because the Al-Ni-rich phase and the Al-(Ni, Co, Cr, Fe) phases have a higher negative mixing enthalpy than the other atom pairs of the five principal elements in the alloy system, and apparently, heat treatment exacerbates this phenomenon [54]. Therefore,

the cooling rate affects not only the phase content and morphology but also the type of microstructure [55].

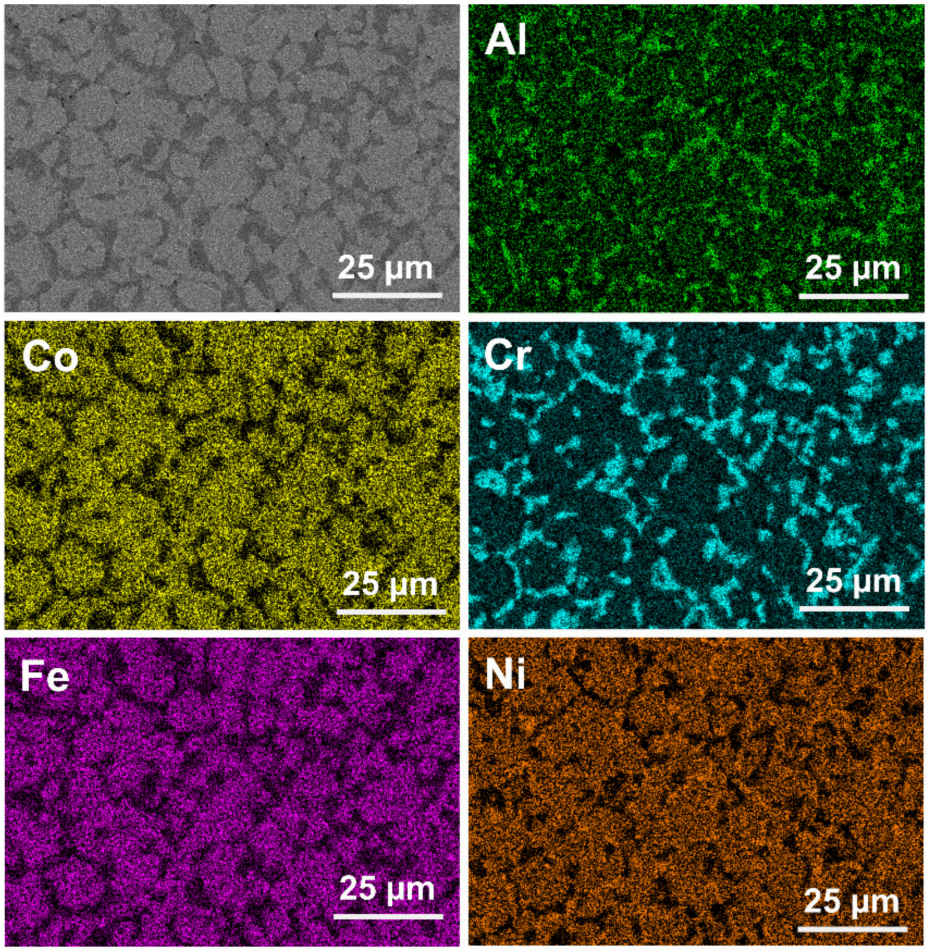

Figure 4. SEM scan results of AC samples. (Al and Ni map, B2 phase; Co, Fe, and Ni map, FCC phase; Cr map, BCC phase).

3.2. Mechanical Properties of Alloys

Figure 5 shows the engineering stress–strain curve of the $Al_{0.5}$CoCrFeNi HEA at room temperature. It can be seen that all the samples undergo plastic deformation, and the tensile strength and yield strength of the samples after heat treatment are significantly increased, and the elongation is decreased. The tensile properties, hardness, and compactness of the alloys are shown in Table 2. The ultimate tensile strength and yield strength of the SS alloy are the lowest, which are 813.8 MPa and 439.5 MPa, respectively, and the elongation is the best, which is 45.7%. The ultimate tensile strength and yield strength of the FC alloy are the highest at 985.2 MPa and 524.1 MPa, and the elongation is the lowest at 36.8%. Compared with the FC and AC alloys, the elongation of the WQ alloy is 43.1% (the least decrease), and the yield strength and ultimate tensile strength (477.5 MPa, 922.2 MPa) are higher than those of the SS alloy (439.5 MPa, 813.8 MPa), so the WQ alloy is a good combination of strength and plasticity. Armin et al. [50] prepared Al0.5CoCrFeNi HEA samples with ultimate tensile strength and yield strength of 1143 MPa and 707 MPa, respectively. However, the elongation is only 21.5%, which is lower than that of our prepared $Al_{0.5}$CoCrFeNi HEA. Compared with other $Al_{0.5}$CoCrFeNi HEA literature reports, the mechanical properties of our prepared samples are superior to them [56–58].

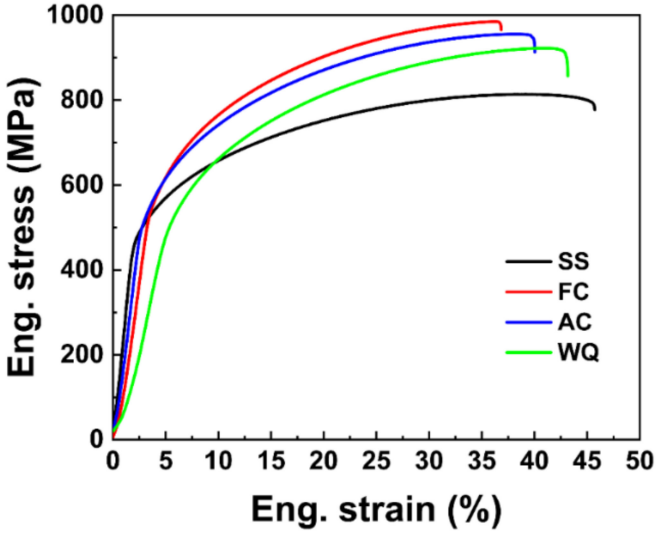

Figure 5. Room-temperature engineering stress–strain curves of $Al_{0.5}$CoCrFeNi HEA as sintered and treated with different cooling rates.

Table 2. Mechanical properties of $Al_{0.5}$CoCrFeNi HEA as sintered and treated with different cooling rates.

Al0.5CoCrFeNi	Yield Strength (MPa)	Ultimate Tensile Strength (MPa)	Elongation (%)	Hardness (HV)	Density (%)
Sintered state	439.5 ± 3	813.8 ± 9	45.7 ± 0.6	267.1 ± 3	99.1 ± 0.6
Furnace cooling	524.1 ± 5	985.2 ± 6	36.8 ± 0.8	393.4 ± 5	99.2 ± 0.8
Air cooling	507.4 ± 3	955.7 ± 8	40.0 ± 1	402.1 ± 9	98.8 ± 1
Water quenched	477.5 ± 2	922.2 ± 4	43.1 ± 0.5	547.3 ± 8	99.3 ± 0.5
Armin et al. [50]	319 ± 10	468 ± 11	30	230 ± 12	-
Jun et al. [56]	707	1143	21.5	-	-
Tong et al. [57]	403	762	37.79	-	-
Niu et al. [58]	360	720	33	-	-

The strength and elongation are related to the phase composition, as shown in Figure 3; after heat treatment, the Cr-rich BCC and Al- and Ni-rich B2 phases increase, while the Co-, Cr-, and Fe-rich FCC phases decrease; the BCC phase structure helps to increase the hardness and strength of the alloy and reduce the ductility of the alloy, while the FCC phase structure is conducive to the development of the alloy with high ductility and low strength [47]. The slip along the (110) plane in the BCC structure is higher than that along the (111) plane in the FCC structure. Slip is much more difficult, so the appearance of B2 phase makes it more difficult to slip, and at the same time, the resistance of dislocation movement increases [59]. Therefore, heat treatment increases the strength of the alloy and reduces the elongation of the alloy.

The hardness of the heat-treated samples is generally higher than that of the SS samples, and with the increase of the cooling rate, the hardness value increases, and the hardness of the WQ alloy reaches 547.3 HV (increased by 280.2 HV compared with the SS alloy). With the acceleration of the cooling rate, the volume of the BCC phase in the alloy becomes larger, resulting in a significant increase in the hardness of the alloy. At the same time, the densities of the alloys in the sintered state and after heat treatment are not much different: both are higher than 98.8%. The BCC and B2 phase structures are precipitated in the FCC matrix of the alloy after heat treatment, thereby increasing the strength of the alloy and reducing the elongation. Further, different cooling rates after heat treatment resulted in different contents of FCC phase, BCC phase, and B2 phase in the alloy, which led to different mechanical properties of alloys with different cooling rates.

Figure 6 shows the tensile fracture morphology of $Al_{0.5}$CoCrFeNi high-entropy alloy. Typical dimple characteristics are observed in all samples, indicating that all alloys have undergone considerable plastic deformation and failed in ductile fracture mode, with an elongation scope from 36.8% to 43.1%, as demonstrated in Table 2. In addition, obvious secondary cracks and micro-cavities can be observed in all the states. The dimples in SS state of Figure 6a are small, and their number density is the largest, which is consistent with the maximum elongation (45.7%). Compared with the SS state in Figure 6a, the dimples of FC and AC in Figure 6b,c are larger, and their number density is smaller, and intergranular fracture can be found in the local region of Figure 6b,c. Moreover, second-phase particles can be seen in the FC and AC alloys in Figure 6b,c respectively, around which voids can form when sufficient stress is applied to break the interfacial bonds between the particle and the matrix, leading to the final fracture [60]. Accordingly, the above two alloys exhibit the worst plasticity: 36.8% and 40%.

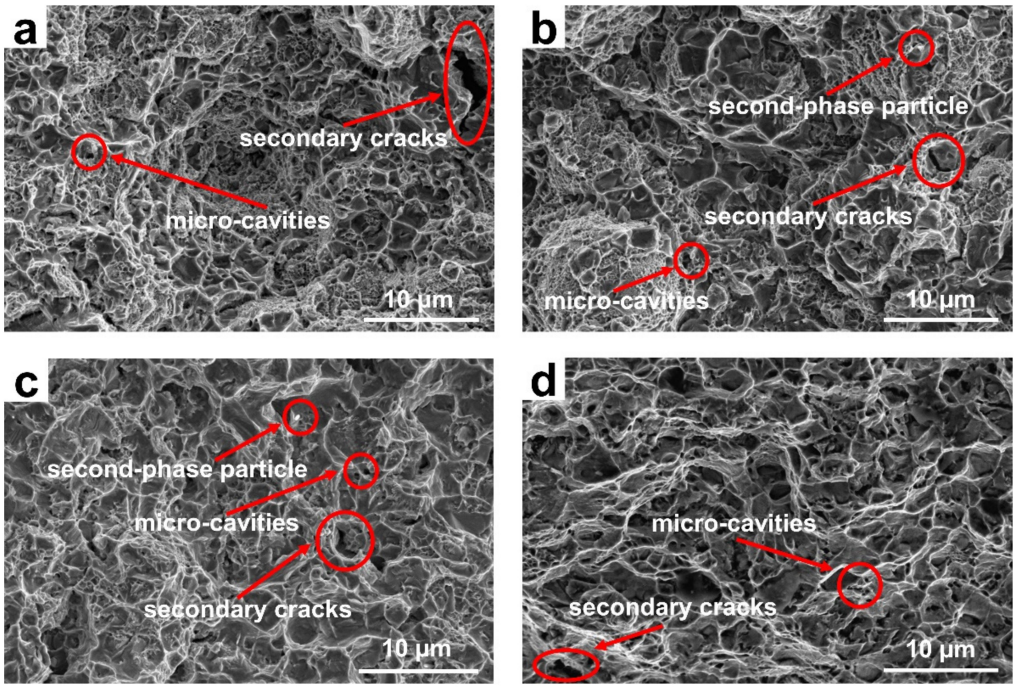

Figure 6. SEM images of tensile fractures of the as-sintered alloys. (**a**) SS and alloys treated with different cooling rates: (**b**) FC; (**c**) AC; (**d**) WQ.

4. Conclusions

In this study, $Al_{0.5}$CoCrFeNi HEA was prepared by SPS technique. The effect of heat-treatment cooling rate on the microstructure and mechanical properties of the alloy was systematically studied, and the results are as follows:

1. The spark plasma sintered sample is composed of BCC + FCC phase, and the sample after heat treatment is composed of B2 + BCC + FCC phase. Heat treatment leads to the transformation of FCC to B2 + BCC phase and, with increasing cooling rate, further coarsening of BCC and B2 phases.
2. The cooling rate has a significant effect on the tensile properties of the samples. The yield strength and ultimate tensile strength of the FC samples reached the highest values of 524.1 MP and 985.2 MPa, and the elongation was 36.8% (8.9% lower than that of the SS samples). The yield strength and ultimate tensile strength of the WQ samples are 477.5 MP and 922.2 MPa, respectively, and the elongation is 43.1% (only 2.6% lower than that of the sintered sample).
3. The hardness of heat-treated samples is higher than that of SS samples, and the hardness value increases with the increase of cooling rate. The hardness of the WQ

sample is 547.3 HV (280.2 HV higher than that of SS sample). The compactness of the samples after heat treatment is above 98.8%.

4. Typical dimple features can be observed in the alloys after heat treatment, indicating that the alloys still have good plastic deformation ability, and their fracture mechanisms are typical plastic fractures.

Author Contributions: Conceptualization, K.X., L.H. and W.F.; methodology, K.X. and L.H.; validation, K.X. and X.W.; formal analysis, L.H., K.X. and L.Y.; investigation, K.X., X.W. and L.Y.; resources, W.F.; data curation, L.H. and K.X.; writing—original draft preparation, K.X. and L.H.; writing—review and editing, K.X., L.H. and X.W.; visualization, W.F.; supervision, W.F. and L.H.; project administration, W.F.; funding acquisition, W.F. and L.H. All authors have read and agreed to the published version of the manuscript.

Funding: This research received no external funding.

Institutional Review Board Statement: Not applicable.

Informed Consent Statement: Not applicable.

Data Availability Statement: Data are contained within the article.

Conflicts of Interest: The authors declare no conflict of interest.

References

1. Tang, Z.; Gao, M.C.; Diao, H.; Yang, T.; Liu, J.; Zuo, T.; Zhang, Y.; Lu, Z.; Cheng, Y.; Zhang, Y. Aluminum alloying effects on lattice types, microstructures, and mechanical behavior of high-entropy alloys systems. *JOM* **2013**, *65*, 1848–1858. [CrossRef]
2. Rao, J.; Diao, H.; Ocelík, V.; Vainchtein, D.; Zhang, C.; Kuo, C.; Tang, Z.; Guo, W.; Poplawsky, J.; Zhou, Y. Secondary phases in alxcocrfeni high-entropy alloys: An in-situ tem heating study and thermodynamic appraisal. *Acta Mater.* **2017**, *131*, 206–220. [CrossRef]
3. Tang, Z.; Senkov, O.N.; Parish, C.M.; Zhang, C.; Zhang, F.; Santodonato, L.J.; Wang, G.; Zhao, G.; Yang, F.; Liaw, P.K. Tensile ductility of an alcocrfeni multi-phase high-entropy alloy through hot isostatic pressing (hip) and homogenization. *Mater. Sci. Eng. A* **2015**, *647*, 229–240. [CrossRef]
4. Shi, Y.; Yang, B.; Xie, X.; Brechtl, J.; Dahmen, K.A.; Liaw, P.K. Corrosion of al x cocrfeni high-entropy alloys: Al-content and potential scan-rate dependent pitting behavior. *Corros. Sci.* **2017**, *119*, 33–45. [CrossRef]
5. Zhao, Y.J.; Qiao, J.W.; Ma, S.G.; Gao, M.C.; Yang, H.J.; Chen, M.W.; Zhang, Y. A hexagonal close-packed high-entropy alloy: The effect of entropy. *Mater. Des.* **2016**, *96*, 10–15. [CrossRef]
6. Santodonato, L.J.; Zhang, Y.; Feygenson, M.; Parish, C.M.; Gao, M.C.; Weber, R.; Neuefeind, J.C.; Tang, Z.; Liaw, P.K. Deviation from high-entropy configurations in the atomic distributions of a multi-principal-element alloy. *Nat. Commun.* **2015**, *6*, 5964. [CrossRef]
7. Gludovatz, B.; Hohenwarter, A.; Catoor, D.; Chang, E.H.; George, E.P.; Ritchie, R.O. Cheminform abstract: A fracture-resistant high-entropy alloy for cryogenic applications. *Sci. Technol. Weld. Join.* **2014**, *345*, 1153. [CrossRef]
8. Li, Z.; Tasan, C.C.; Pradeep, K.G.; Raabe, D. A trip-assisted dual-phase high-entropy alloy: Grain size and phase fraction effects on deformation behavior. *Acta Mater.* **2017**, *131*, 323–335. [CrossRef]
9. Chuang, M.H.; Tsai, M.H.; Tsai, C.W.; Yang, N.H.; Chang, S.Y.; Yeh, J.W.; Chen, S.K.; Lin, S.J. Intrinsic surface hardening and precipitation kinetics of al0.3crfe1.5mnni0.5 multi-component alloy. *J. Alloys Compd.* **2013**, *551*, 12–18. [CrossRef]
10. Li, R.; Niu, P.; Yuan, T.; Cao, P.; Chen, C.; Zhou, K. Selective laser melting of an equiatomic cocrfemnni high-entropy alloy: Processability, non-equilibrium microstructure and mechanical property. *J. Alloys Compd.* **2018**, *746*, 125–134. [CrossRef]
11. Wu, W.; Song, M.; Ni, S.; Wang, J.; Liu, Y.; Liu, B.; Liao, X. Dual mechanisms of grain refinement in a fecocrni high-entropy alloy processed by high-pressure torsion. *Sci. Rep.* **2017**, *7*, 1–13. [CrossRef] [PubMed]
12. Xiao, D.H.; Zhou, P.F.; Wu, W.Q.; Diao, H.Y.; Gao, M.C.; Song, M.; Liaw, P.K. Microstructure, mechanical and corrosion behaviors of alcocufeni-(cr,ti) high entropy alloys. *Mater. Des.* **2017**, *116*, 438–447. [CrossRef]
13. Cantor, B.; Chang, I.; Knight, P.; Vincent, A. Microstructural development in equiatomic multicomponent alloys. *Mater. Sci. Eng. A* **2004**, *375–377*, 213–218. [CrossRef]
14. Yeh, J.-W.; Chen, S.-K.; Lin, S.-J.; Gan, J.-Y.; Chin, T.-S. Nanostructured high-entropy alloys with multiple principal elements: Novel alloy design concepts and outcomes. *Adv. Eng. Mater.* **2004**, *6*, 299–303. [CrossRef]
15. Yong, Z.A.; Ttz, A.; Zhi, T.B.; Mcgc, D.; Kad, E.; Pkl, B.; Zhao, P. Microstructures and properties of high-entropy alloys. *Prog. Mater Sci.* **2014**, *61*, 1–93.
16. Butler, T.M.; Weaver, M.L. Investigation of the phase stabilities in alnicocrfe high entropy alloys. *J. Alloys Compd.* **2017**, *691*, 119–129. [CrossRef]
17. Lee, K.S.; Kang, J.H.; Lim, K.R.; Na, Y.S. Influence of compressive strain on the microstructural evolution of an alcocrfeni high entropy alloy. *Mater. Charact.* **2017**, *132*, 162–168. [CrossRef]

18. Wang, W.R.; Wang, W.L.; Yeh, J.W. Phases, microstructure and mechanical properties of alxcocrfeni high-entropy alloys at elevated temperatures. *J. Alloys Compd.* **2014**, *589*, 143–152. [CrossRef]
19. Zhou, P.; Xiao, D.H.; Wu, Z.; Song, M. Microstructure and mechanical properties of alcocrfeni high entropy alloys produced by spark plasma sintering. *Mater. Res. Express* **2019**, *6*, 0865e7. [CrossRef]
20. Wang, F.J.; Zhang, Y.; Chen, G.L.; Davies, H.A. Cooling rate and size effect on the microstructure and mechanical properties of alcocrfeni high entropy alloy. *J. Eng. Mater. Technol.* **2009**, *131*, 034501. [CrossRef]
21. Butler, T.M.; Weaver, M.L. Oxidation behavior of arc melted alcocrfeni multi-component high-entropy alloys. *J. Alloys Compd.* **2016**, *647*, 229–244. [CrossRef]
22. Karlsson, D.; Lindwall, G.; Lundbäck, A.; Amnebrink, M.; Boström, M.; Riekehr, L.; Schuisky, M.; Sahlberg, M.; Jansson, U. Binder jetting of the alcocrfeni alloy. *Addit. Manuf.* **2019**, *27*, 72–79. [CrossRef]
23. Uporov, S.; Bykov, V.; Pryanichnikov, S.; Shubin, A.; Uporova, N. Effect of synthesis route on structure and properties of alcocrfeni high-entropy alloy. *Intermetallics* **2017**, *83*, 1–8. [CrossRef]
24. Muthupandi, G.; Lim, K.R.; Na, Y.S.; Park, J.; Lee, D.; Kim, H.; Park, S.; Choi, Y.S. Pile-up and sink-in nanoindentation behaviors in alcocrfeni multi-phase high entropy alloy. *Mater. Sci. Eng. A* **2017**, *696*, 146–154. [CrossRef]
25. Wu, Z.; Bei, H.; Otto, F.; Pharr, G.M.; George, E.P. Recovery, recrystallization, grain growth and phase stability of a family of fcc-structured multi-component equiatomic solid solution alloys. *Intermetallics* **2014**, *46*, 131–140. [CrossRef]
26. Li, Y.; Lee, J.; Kang, B.; Hong, S.H. Microstructure and elevated-temperature mechanical properties of refractory almo0.5nbta0.5tizr high entropy alloy fabricated by powder metallurgy. *arXiv* **2017**, arXiv:1801.00263.
27. Ji, W.; Wang, W.; Wang, H.; Zhang, J.; Wang, Y.; Zhang, F.; Fu, Z. Alloying behavior and novel properties of cocrfenimn high-entropy alloy fabricated by mechanical alloying and spark plasma sintering. *Intermetallics* **2015**, *56*, 24–27. [CrossRef]
28. Zhang, M.; Li, R.; Yuan, T.; Feng, X.; Xie, S. Effect of low-melting-point sintering aid on densification mechanisms of boron carbide during spark plasma sintering. *Scripta Mater.* **2019**, *163*, 34–39. [CrossRef]
29. Deng, S.; Li, R.; Yuan, T.; Xie, S.; Zhang, M.; Zhou, K.; Cao, P. Direct current-enhanced densification kinetics during spark plasma sintering of tungsten powder. *Scripta Mater.* **2018**, *143*, 25–29. [CrossRef]
30. Zhang, M.; Yuan, T.; Li, R.; Xie, S.; Wang, M.; Weng, Q. Densification mechanisms and microstructural evolution during spark plasma sintering of boron carbide powders. *Ceram. Int.* **2018**, *44*, 3571–3579. [CrossRef]
31. Liu, G.; Li, R.; Yuan, T.; Zhang, M.; Zeng, F. Spark plasma sintering of pure ticn: Densification mechanism, grain growth and mechanical properties. *Int. J. Refract. Met. Hard Mater.* **2017**, *66*, 68–75. [CrossRef]
32. Guillon, O.; Gonzalez-Julian, J.; Dargatz, B.; Kessel, T.; Schierning, G.; Räthel, J.; Herrmann, M. Field-assisted sintering technology/spark plasma sintering: Mechanisms, materials, and technology developments. *Adv. Eng. Mater.* **2014**, *16*, 830–849. [CrossRef]
33. Giuntini, D.; Olevsky, E.A.; Garcia-Cardona, C.; Maximenko, A.L.; Yurlova, M.S.; Haines, C.D.; Martin, D.G.; Kapoor, D. Localized overheating phenomena and optimization of spark-plasma sintering tooling design. *Materials* **2013**, *6*, 2612–2632. [CrossRef] [PubMed]
34. Zhang, A.; Han, J.; Meng, J.; Su, B.; Li, P. Rapid preparation of alcocrfeni high entropy alloy by spark plasma sintering from elemental powder mixture. *Mater. Lett.* **2016**, *181*, 82–85. [CrossRef]
35. Mohanty, S.; Maity, T.N.; Mukhopadhyay, S.; Sarkar, S.; Gurao, N.P. Powder metallurgical processing of equiatomic alcocrfeni high entropy alloy: Microstructure and mechanical properties. *Mater. Sci. Eng. A* **2017**, *679*, 299–313. [CrossRef]
36. Shivam, V.; Shadangi, Y.; Basu, J.; Mukhopadhyay, N.K. Evolution of phases, hardness and magnetic properties of alcocrfeni high entropy alloy processed by mechanical alloying. *J. Alloys Compd.* **2020**, *832*, 154826. [CrossRef]
37. Vaidya, M.; Muralikrishna, G.M.; Murty, B.S. High-entropy alloys by mechanical alloying: A review. *J. Mater. Res.* **2019**, *34*, 664–686. [CrossRef]
38. Kunce, I.; Polanski, M.; Karczewski, K.; Plocinski, T.; Kurzydlowski, K.J. Microstructural characterisation of high-entropy alloy alcocrfeni fabricated by laser engineered net shaping. *J. Alloys Compd.* **2015**, *648*, 751–758. [CrossRef]
39. Xie, S.; Li, R.; Yuan, T.; Zhang, M.; Cao, P. Effect of phase transformation on densification kinetics and properties of spark plasma sintered al0.7cocrfeni high-entropy alloy. *Mater. Charact.* **2019**, *160*, 110098. [CrossRef]
40. Yang, T.; Xia, S.; Liu, S.; Wang, C.; Wang, Y. Effects of al addition on microstructure and mechanical properties of alxcocrfeni high-entropy alloy. *Mater. Sci. Eng. A* **2015**, *648*, 15–22. [CrossRef]
41. Kattner, U.R. The thermodynamic modeling of multicomponent phase equilibria. *JOM* **1997**, *49*, 14–19. [CrossRef]
42. Kube, S.A.; Schroers, J. Metastability in high entropy alloys. *Scripta Mater.* **2020**, *186*, 392–400. [CrossRef]
43. Feng, Y.; Qiu, T. Preparation, characterization and microwave absorbing properties of feni alloy prepared by gas atomization method. *J. Alloys Compd.* **2012**, *513*, 455–459. [CrossRef]
44. Zhang, J.; Wang, B.; Yao, C. Comparative study of in600 superalloy produced by two powder metallurgy technologies: Argon atomizing and plasma rotating electrode process. *Vacuum* **2018**, *156*, 302–309.
45. Gao, C.-f.; Xiao, Z.-y.; Zou, H.-p.; Liu, Z.-q.; Jin, C.; Li, S.-k.; Zhang, D.-t. Characterization of spherical alsi10mg powder produced by double-nozzle gas atomization using different parameters. *Trans. Nonferrous Met. Soc. China* **2019**, *29*, 374–384. [CrossRef]
46. Munitz, A.; Salhov, S.; Hayun, S.; Frage, N. Heat treatment impacts the micro-structure and mechanical properties of alcocrfeni high entropy alloy. *J. Alloys Compd.* **2016**, *683*, 221–230. [CrossRef]

47. Kao, Y.F.; Chen, T.J.; Chen, S.K.; Yeh, J.W. Microstructure and mechanical property of as-cast, -homogenized, and -deformed alxcocrfeni (0 <= x <= 2) high-entropy alloys. *J. Alloys Compd.* **2009**, *488*, 57–64. [CrossRef]
48. Ji, W.; Fu, Z.; Wang, W.; Wang, H.; Zhang, J.; Wang, Y.; Zhang, F. Mechanical alloying synthesis and spark plasma sintering consolidation of cocrfenial high-entropy alloy. *J. Alloys Compd.* **2014**, *589*, 61–66. [CrossRef]
49. Zhang, Y.; Li, J.; Wang, J.; Niu, S.; Kou, H. Hot deformation behavior of as-cast and homogenized al0.5cocrfeni high entropy alloys. *Metals* **2016**, *6*, 277. [CrossRef]
50. Ghaderi, A.; Moghanni, H.; Dehghani, K. Microstructural evolution and mechanical properties of al0.5cocrfeni high-entropy alloy after cold rolling and annealing treatments. *J. Mater. Eng. Perform.* **2021**, *30*, 7817–7825. [CrossRef]
51. Zhou, P.F.; Xiao, D.H.; Yuan, T.C. Microstructure, mechanical and corrosion properties of alcocrfeni high-entropy alloy prepared by spark plasma sintering. *Acta Metall. Sin. (Engl. Lett.)* **2020**, *33*, 937–946. [CrossRef]
52. Aizenshtein, M.; Priel, E.; Hayun, S. Effect of pre-deformation and b2 morphology on the mechanical properties of al0. 5cocrfeni hea. *Mater. Sci. Eng. A* **2020**, *788*, 139575. [CrossRef]
53. Wrwa, B.; Wlw, B.; Scw, B.; Yct, B.; Chl, B.; Jwy, A. Effects of al addition on the microstructure and mechanical property of al x cocrfeni high-entropy alloys. *Intermetallics* **2012**, *26*, 44–51.
54. Lin, C.M.; Tsai, H.L. Evolution of microstructure, hardness, and corrosion properties of high-entropy al0.5cocrfeni alloy. *Intermetallics* **2011**, *19*, 288–294. [CrossRef]
55. Lv, Y.; Hu, R.; Yao, Z.; Chen, J.; Xu, D.; Liu, Y.; Fan, X. Cooling rate effect on microstructure and mechanical properties of al x cocrfeni high entropy alloys. *Mater. Des.* **2017**, *132*, 392–399. [CrossRef]
56. Wang, J.; Niu, S.; Guo, T.; Kou, H.; Li, J. The fcc to bcc phase transformation kinetics in an al 0.5 cocrfeni high entropy alloy. *J. Alloys Compd.* **2017**, *710*, 144–150. [CrossRef]
57. Guo, T.; Li, J.; Wang, J.; Wang, W.Y.; Liu, Y.; Luo, X.; Kou, H.; Beaugnon, E. Microstructure and properties of bulk al 0.5 cocrfeni high-entropy alloy by cold rolling and subsequent annealing. *Mater. Sci. Eng. A* **2018**, *729*, 141–148. [CrossRef]
58. Niu, S.Z.; Kou, H.C.; Wang, J.; Li, J.S. Improved tensile properties of al0.5cocrfeni high-entropy alloy by tailoring microstructures. *Rare Met.* **2021**, *40*, 1–6. [CrossRef]
59. Tang, Q.H.; Zhao, Y.G.; Cai, J.B.; Dai, P.Q. Effect of aging treatment on microstructures and mechanical properties of al0.5cocrfeni high-entropy alloy. *Trans. Nonferrous Met. Soc. China* **2011**, *4*, 47–50.
60. Xu, D.; Chen, K.; Chen, Y.; Chen, S. Evolution of the second-phase particles and their effect on tensile fracture behavior of 2219 al-xcu alloys. *Metals* **2020**, *10*, 197. [CrossRef]